THE ASTROPHYSICAL JOURNAL, 462:364–375, 1996 May 1

THE STRUCTURE AND THERMAL EVOLUTION OF STRANGE DWARF STARS

O. G. BENVENUTO[1] AND L. G. ALTHAUS[2]
Facultad de Ciencias Astronómicas y Geofísicas, Universidad Nacional de La Plata, Paseo del Bosque S/N, (1900) La Plata, Argentina;
obenvenuto, althaus@fcaglp.fcaglp.unlp.edu.ar
Received 1995 September 11; accepted 1995 November 20

ABSTRACT

We study the structure and evolution of strange dwarf stars: stellar objects composed of a compact core made up of strange matter surrounded by a normal matter envelope, which at its bottom has a density lower than or equal to that of the neutron drip. We restrict our analysis to the case of low–central pressure objects that have a mass-radius relation very similar to the corresponding to white dwarf stars.

We show by means of a simplified analysis that strange dwarfs resembling white dwarfs correspond to a very narrow range of central pressures. The almost discontinuous behavior of these structures with respect to changes of the central pressure is studied by means of a polytropic-like analysis, which shows that the envelope of all these objects is well described by the Lane-Emden equation with $n = 3$ but with boundary conditions different from the ordinary ones. In contrast to earlier expectations, we show that strange dwarf stars are stable only if the density at the bottom of the normal matter envelope is lower than that of the neutron drip.

We have computed the evolution of strange dwarf stars of 0.4, 0.55, and 0.8 $M_\odot$ in the range of luminosities usually attributed to white dwarf stars. Because of the lack of computations of the previous evolution for such objects, two types of chemical composition were assumed: carbon-oxygen up to a density ρ of $\rho = 10^9$ g cm^{-3} (type A models) and up to $\rho = 10^7$ g cm^{-3} (type B models), respectively. For higher densities, we assumed nuclear statistical equilibrium. We show the central and maximum temperature, neutrino emission, crystallization profile, ages, and the luminosity function versus the stellar luminosity for each type of model and each stellar mass. We found that if the density at the base of the normal matter envelope is slightly lower than that of neutron drip, these objects have a luminosity function observationally indistinguishable from the corresponding luminosity function in white dwarf stars. This is independent of the chemical composition of the normal matter, high-density layers. Thus, the observational data on the cooling of white dwarfs are not in contradiction with the strange matter hypothesis. However, strange dwarfs should behave very differently from white dwarfs in mass-exchanging close binary systems.

Subject headings: dense matter — elementary particles — stars: interiors — white dwarfs

1. INTRODUCTION

The possibility of the absolute stability of strange matter (an almost symmetric plasma of u, d, and s quarks, hereafter SM) has been extensively explored since the seminal paper of Witten (1984). Because SM is expected to occur in extreme conditions, research has been mostly addressed to the role of SM in cosmology and astrophysics. At present it is known that if the SM conjecture is indeed correct, nucleation of SM is very probable in the dense interior of neutron stars (Horvath, Benvenuto, & Vucetich 1992; Olesen & Madsen 1994), and, consequently, most of the stars currently believed to be neutron stars should be strange stars (SSs) (Alcock & Olinto 1988; Benvenuto, Horvath, & Vucetich 1991). Moreover, it seems possible that SM formation prompts Type II supernova explosions (Benvenuto, Horvath, & Vucetich 1989; Benvenuto & Horvath 1989; Benvenuto et al. 1991). For general reference to the early works on SM, see Madsen & Haensel (1991).

More recently, efforts have been focused on the equation of state (EOS) of SM. It has been recently shown by Benvenuto & Lugones (1995) and Lugones & Benvenuto (1995a) that, despite earlier expectations (see, e.g., Chakrabarty, Raha, & Sinha 1989), in the quark mass density–dependent model, the SM EOS is very similar to that predicted by the MIT bag model. This is verified at $T = 0$ as well as at $T > 0$. Additionally, the transport properties of quark-gluon plasmas at finite temperature have been analyzed in a very general framework by Heiselberg & Pethick (1993).

In order to shed light on what we would have to look for to detect SM in heavy ion collisions, Lee & Heinz (1993) have studied the phase structure of SM and the possibility of the formation of metastable strangelets. On the other hand, the combustion of nuclear matter into SM has been studied in, for example, Lugones, Benvenuto, & Vucetich (1994) and Lugones & Benvenuto (1995b). Such a process should be very important in the dynamics of a growing SM core in a stellar environment, for example, in supernovae (Benvenuto & Horvath 1989).

Very recently, Glendenning, Kettner, & Weber (1995a) (hereafter GKW; see also Glendenning, Kettner, & Weber 1995b) have proposed another kind of astrophysical object involving SM: stellar configurations with a small, dense SM core surrounded by an extended, normal matter envelope, which at its bottom has a density ρ_B equal to that of the neutron drip $\rho_{\rm drip} = 4 \times 10^{11}$ g cm^{-3}. This is the highest density for normal matter and SM coexistence to be possible (Alcock & Olinto 1988). In GKW, authors have solved the equations for radial pulsations in the frame of general

[1] Member of the Carrera del Investigador Científico, Comisión de Investigaciones Científicas de la Provincia de Buenos Aires (CIC), Argentina.
[2] Fellow of the Consejo Nacional de Investigaciones Científicas y Técnicas (CONICET), Argentina.

relativity (Chandrasekhar 1964) and have found that these objects are stable against radial perturbations and thus may exist. Nevertheless, as discussed in § 4, they have ignored the effect of the variation of the density induced by the pulsations themselves, which destabilize objects with $\rho_B = \rho_{\rm drip}$ but do not destabilize objects with $\rho_B \lesssim \rho_{\rm drip}$. Such objects have been called strange dwarf (SD) stars.

From the astrophysical point of view, in the regime of low central pressures, SDs resemble the well-known white dwarf (WD) stars (for earlier discussion about the relation between WDs and SSs, see also Alcock & Olinto 1988). Because of the very similar mass-radius relationships, SDs are in principle very difficult to distinguish from WDs. A way to perform such a differentiation may be to study the cooling of both kinds of objects and to compare them with each other and with observations as well. It is the aim of this work to perform a detailed evolutionary study of SDs and to analyze the viability of such a test for differentiation. A short account of the main results of this work has already been presented in Benvenuto & Althaus (1995b).

We should note that in order to make this approach powerful, we should be able to calculate the relative fraction of the normal WD and SD population. This is not possible at present. Nevertheless, if the evolution of WDs and SDs were very different, observable evolutionary differences should be detectable in, for example, galactic open clusters, where objects share many common features (such as their ages).

In § 2 we discuss the properties of SM that we incorporated in our code. The general properties of the structure of SD stars are addressed in § 3, where we present a study based on a polytropic-like analysis. We discuss the validity of the stability analysis for SDs performed in GKW in § 4. The problem of the composition of the normal matter envelope of SD is addressed in § 5. The numerical code we employed is described in § 6. In § 7, we present the method for constructing the initial SD models and the cooling calculations. Finally, in § 8 we present a discussion and the main conclusions of this work.

2. THE PROPERTIES OF STRANGE MATTER

In order to describe SM we adopted the EOS of the MIT bag model (see, e.g., Farhi & Jaffe 1984),

$$P = \tfrac{1}{3}(\rho c^2 - 4B)\,, \tag{1}$$

where B is the bag constant, for which we assumed the typical value of $B = 60$ MeV fm^{-3}. We have adopted only one value for the parameter B because the structure of SDs is almost insensitive to variations of this quantity. SSs are indeed sensitive to the value of B, but this topic has been widely discussed in the literature and we shall not address it here (see, e.g., Witten 1984; Benvenuto et al. 1991).

For the thermal conductivity $\kappa_{\rm cond}$ and neutrino emissivity ϵ_β of SM, we adopted the expressions given by Heiselberg & Pethick (1993)

$$\kappa_{\rm cond} = 9.79 \times 10^{21}\left(\frac{\alpha_c}{0.1}\right)^{-1}\left(\frac{\mu}{300\ {\rm MeV}}\right)^2 \frac{\rm ergs}{\rm cm\ s\ K} \tag{2}$$

and Haensel (1991)

$$\epsilon_\beta = 2.2 \times 10^{26}\alpha_c Y_e^{1/3} T_9^6 \frac{n}{n_0}\frac{\rm ergs}{\rm cm^3\ s\ K}\,, \tag{3}$$

respectively, where α_c is the QCD coupling, μ is the quark chemical potential, Y_e is the number of electrons per baryon, T_9 is the temperature in units of 10^9 K, and n (n_0) is the baryon (saturation) density. In the present work we assumed the typical values of $\mu = 278$ MeV, $\alpha_c = 0.1$, and $Y_e = 10^{-3}$. It will be clear in § 7.2 that $\kappa_{\rm cond}$ is so high that it is unnecessary to know it with high accuracy for our purposes. Also, note that the exact value of $\alpha_c Y_e^{1/3}$ is strongly dependent upon the exact value of the mass of the strange quark (Farhi & Jaffe 1984), which is poorly known at present, and the assumed value of 10^{-2} represents an upper limit for $\alpha_c Y_e^{1/3}$ and accordingly gives an upper limit for ϵ_β.

3. THE STRUCTURE OF STRANGE DWARF STARS

In this work we are interested in the properties of SDs of low central pressure P_c (i.e., the objects that resemble WDs). As in these cases $P_c \ll B$, it is highly accurate to consider the SM core as a constant-density sphere. This (central) density ρ_c is $\rho_c = 4B/c^2 = 4.26 \times 10^{14}$ g cm^{-3}. In this approximation, neglecting $P_{\rm drip}$ ($P_{\rm drip} \ll P_c$), the radius and mass of the SM core are

$$R_{\rm SM} = \left(\frac{3P_c}{2\pi G\rho_c^2}\right)^{1/2}, \tag{4}$$

and

$$M_{\rm SM} = \left(\frac{6}{\pi}\right)^{1/2}\left(\frac{P_c}{G}\right)^{3/2}\rho_c^{-2}\,. \tag{5}$$

Surrounding the SM core, there is an extended normal matter envelope, whose bottom is at $\rho_B \lesssim \rho_{\rm drip}$. For the purposes of this section, an accurate knowledge of ρ_B is unnecessary, so we shall assume $\rho_B \leq \rho_{\rm drip}$ in spite of the discussion of § 4. Let us, for the sake of simplicity and only in this section, neglect the modifications to the structure induced by the presence of heavy elements in the high-density, normal matter layers as well as the corrections to the EOS due to Coulomb interactions, etc. (Salpeter 1961). Then, the EOS for the envelope is (Chandrasekhar 1939)

$$P = A[x(x^2+1)^{1/2}(2x^2-3) + 3\sin h^{-1}(x)] \tag{6}$$

$$\rho = Cx^3\,, \tag{7}$$

where $A = \pi m_e^4 c^5/3h^3$ and $C = 8\pi m_e^3 c^3 \mu_e M_u/3h^3$ (the symbols have their usual meanings).

If we apply the equations of structure for such an envelope, it can be straightforwardly verified that it fulfills the famous Chandrasekhar (1939) equation

$$\frac{1}{\eta^2}\frac{d}{d\eta}\left(\eta^2\frac{d\phi}{d\eta}\right) = -\left(\phi^2 - \frac{1}{y_B^2}\right)^{3/2}, \tag{8}$$

where $\phi = y/y_B$, $y = (1+x^2)^{1/2}$, y_B is related to ρ_B via equation (7), and $\eta = r/\alpha$ with α given by

$$\alpha = \left(\frac{2A}{\pi G}\right)^{1/2}\frac{1}{Cy_B}\,. \tag{9}$$

The density can be expressed as

$$\rho = Cy_B^3\left(\phi^2 - \frac{1}{y_B^2}\right)^{3/2}. \tag{10}$$

For $\rho_B = \rho_{\rm drip}$ we have $y_B \approx 60$, so that if we neglect terms of order y_B^{-2}, equation (8) reduces to the Lane-Emden equation of index $n = 3$ with $\phi = (\rho/\rho_B)^{1/3}$ for *all* these objects.

Of course, the boundary conditions are not the usual ones. First of all, if we take $\rho = \rho_B$, then, at $r = R_{SM}$ ($\eta_{SM} = R_{SM}/\alpha$),

$$\phi(\eta_{SM}) = 1 . \tag{11}$$

Let us calculate the value of the derivative of ϕ at $r = R_{SM}$. Employing equation (7), we have

$$\frac{d\rho}{dr} = \frac{3\rho_{drip}}{\alpha}\frac{d\phi}{d\eta} , \tag{12}$$

and imposing hydrostatic equilibrium

$$\frac{dx}{dr} = -\left(\frac{GM}{R^2}\right)_{SM}\frac{C}{8A} , \tag{13}$$

which neglecting terms of order y_B^2 and after some arrangement gives

$$\phi'(\eta_{SM}) \equiv \left.\frac{d\phi}{d\eta}\right|_{\eta=\eta_{SM}} = -\frac{1}{2y_B^2}\left(\frac{P_c}{3A}\right)^{1/2} = -\left(\frac{P_c}{6P_{drip}}\right)^{1/2} . \tag{14}$$

In the case in which we are interested in this work, we have, from our numerical models, $P_c \approx 2$ MeV fm^{-3} and $P_{drip} \approx 10^{-3}$ MeV fm^{-3}, and then $\eta_{SM} \approx 0.038$ and $\phi'(\eta_{SM}) \approx 20$.

The expression for the total mass of the structure (including the SM core) is given by

$$M = \frac{4\pi}{C^2}\left(\frac{2A}{\pi G}\right)^{3/2}\left(-\eta^2\frac{d\phi}{d\eta}\right)\Big|_{\eta=\eta_1} , \tag{15}$$

where, as usual, η_1 is the coordinate at which density vanishes.

We show ϕ and $-\eta^2 d\phi/d\eta$ versus η in Figures 1 and 2, respectively. To achieve this, we have integrated the Lane-Emden equation of $n = 3$ for $\phi(\eta_{SM}) = 1$ and values of the derivative at $\eta_{SM} = 0.038$ varying from 0 to 30 in steps of 1.

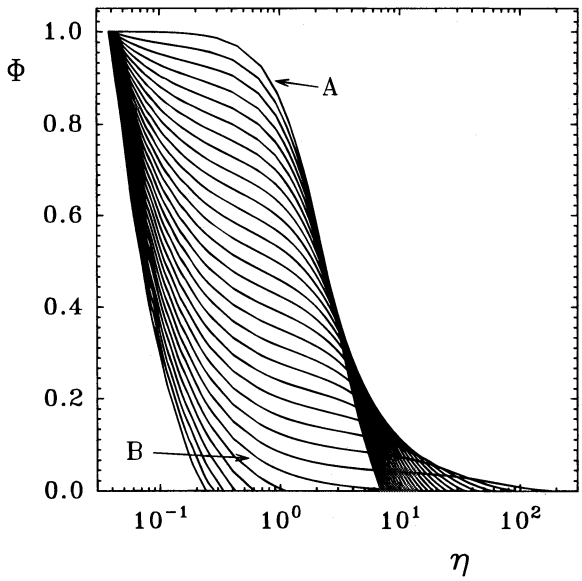

FIG. 1.—Solution of the Lane-Emden equation for $n = 3$ for derivatives at $\eta_{SM} = 0.038$ varying from 0 to 30 with steps of 1. Curve A corresponds to $\phi'(\eta_{SM}) = 0$. Note that at $\phi'(\eta_{SM}) \approx 24$ (curve B), the radius of the sphere is a steeply decreasing function of $\phi'(\eta_{SM})$. This corresponds to a central pressure $P_c = 3.4$ MeV fm^{-3}, in agreement with our numerical calculation.

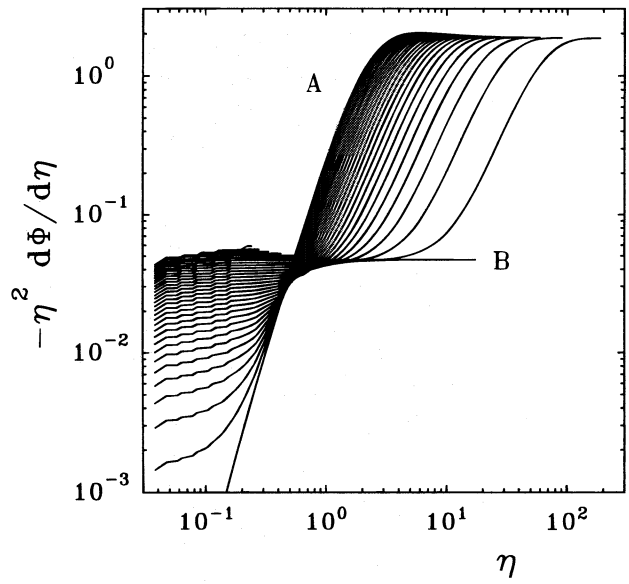

FIG. 2.—Minus the derivative of the Lane-Emden function for $n = 3$ times the square of the radius for derivatives at origin varying from 0 to 30 at steps of 1. Curves are labeled as in Fig. 1.

The solution with $\phi'(\eta_{SM}) = 0$, labeled as A, is the nearest to the normal one [$\phi(0) = 1$, $\phi'(0) = 0$]. It can be realized from Figure 1 that, in a narrow range of central densities, the radius of the structure is a steeply decreasing function of $\phi'(\eta_{SM})$. This behavior is found in a narrow interval of central pressures just higher than that corresponding to curve B, for which our analytical model gives $P_c \approx 3.4$ MeV fm^{-3}.

For the sake of completeness, we show in Figure 3 the mass-radius relationship resulting from integrating the general relativistic Oppenheimer & Volkoff (1939) equations of stellar structure with the EOSs given by equations (1) and (6)–(7). The corresponding behavior of the central pressure with the stellar mass and with M_{SM} and R_{SM} are shown in Figures 4 and 5, respectively. In addition, we incorporated in Figure 5 the analytical approximations to R_{SM} and M_{SM}, equations (4) and (5), showing that they are in very good agreement with numerical integrations. In fact, the constant-density approximation breaks down for central pressures $P_c \geq 10$ MeV fm^{-3}, i.e., pressures comparable with the value of the bag constant B.

In Figures 3, 4, and 5, we have also included, with dotted lines, the resulting structure of SDs if we change the value of the bag constant B to the value of $B = 80$ MeV fm^{-3}, which represents SM less strongly bounded than with $B = 60$ MeV fm^{-3}. Note that the structure of SDs we are interested in here shows little sensitivity to B, which justifyies the use of only one value as quoted in § 2.

It is clear from Figure 4 that WD-like objects lie in a very narrow range of central pressures that just correspond to those values of P_c of the "critical" polytrope (see curve B of Fig. 1). This almost discontinuous characteristic is nicely accounted for by the behavior of the function ϕ with changes in P_c (eq. [14]) for $P_c \gtrsim 3.4$ MeV fm^{-3} [$\phi'(\eta_{SM}) \gtrsim 24$]. It is important for the following discussion to note that for SDs that resemble WDs, the larger the stellar mass, the smaller the SM core is.

It can be realized from Figure 3 that the heaviest SD star models we found correspond (almost independent of the

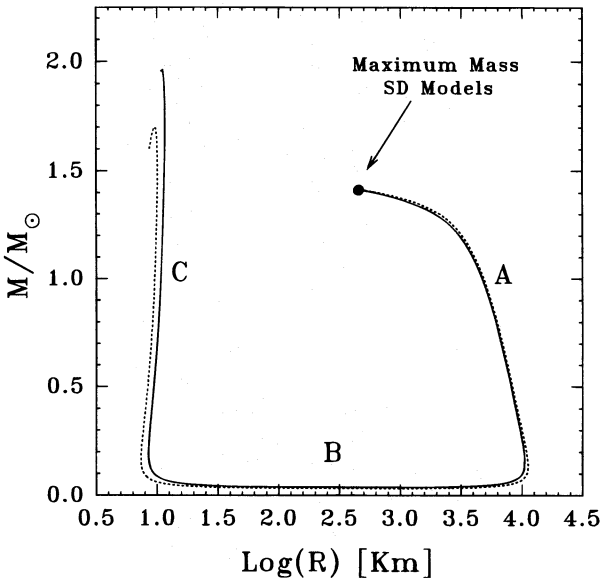

FIG. 3.—Stellar mass vs. radius relationship for SD stars resulting from the integration of the Oppenheimer & Volkoff (1939) equations together with the EOSs given by eqs. (1) and (6)–(7). The objects labeled as A and C resemble normal WDs and SSs, respectively, whereas the rest of the curve (B) corresponds to low-mass SDs. Dotted lines represent the results corresponding to a value of the bag constant B of $B = 80$ MeV fm^{-3}. For these models we have assumed $\rho_B = \rho_{drip}$. Note, however, that for our evolutionary models we considered the case of $\rho_B = 0.9\rho_{drip}$ (see text for explanation). Maximum masses of SD models are denoted with filled dots and are almost the same for both sequences.

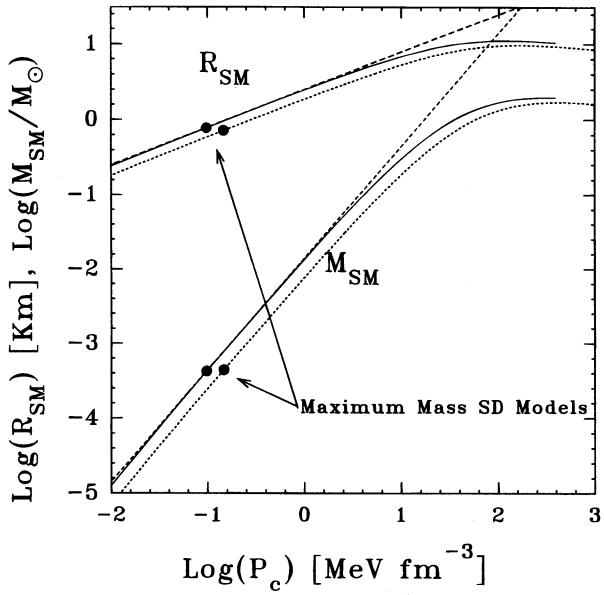

FIG. 5.—Mass and radius of the SM core vs. central pressure for SD stars. Note that these curves have no discontinuity. The approximate expressions for constant-density SM core (eqs. [4] and [5], assuming $B = 60$ MeV fm^{-3}) are shown as short dashed lines. Note that this approximation is excellent up to $P_c \approx 10$ MeV fm^{-3}. This pressure corresponds to low-mass SSs. Dotted lines have the same meaning as in Fig. 3. Maximum mass SD models of both sequences are denoted with filled dots.

value of the bag constant B) to a mass and radius of $M = 1.41210\ M_\odot$ (very near the Chandrasekhar mass) and log R [km] = 2.6526. GKW found the heaviest SD model to have $M = 0.93\ M_\odot$ and log R [km] = 3.398. Such differences can be traced back to the different treatments of the EOS between GKW and the present paper. GKW found values very close to those corresponding to the heaviest WD made up of matter in nuclear statistical equilibrium (see Shapiro & Teukolsky 1983), which is not surprising because they employed the equilibrium EOS of Baym, Pethick, Sutherland (1971). However, in this section we used the EOS given by equations (6)–(7) that, for WD models, gives a maximum mass star of zero radius (Chandrasekhar 1939). So, it is clear that the differences we found in mass and radius for the heaviest SD object are due to the EOS assumptions.

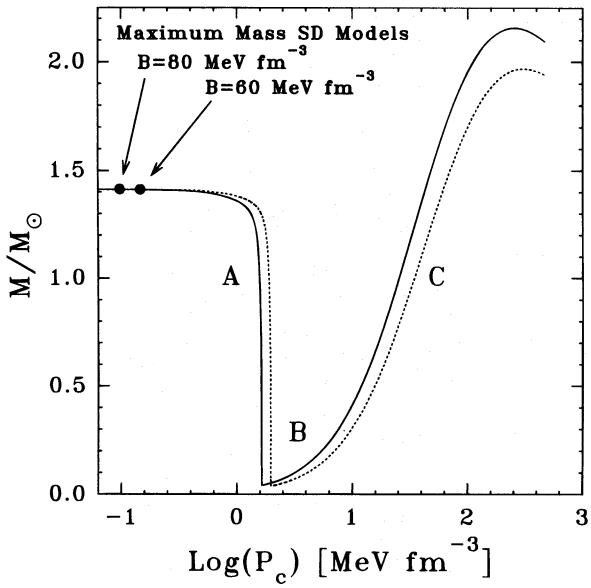

FIG. 4.—Stellar mass vs. central pressure relationship for SD stars. SDs resembling WDs correspond to the steeply decreasing part (A) of the curve. Note that, in this part of the curve, the larger the stellar mass, the lower the central pressure. Very low mass SDs correspond to the deep minimum (B), whereas the object resembling SSs correspond to the rest of the curve (C). Dotted lines have the same meaning as in Fig. 3. For these models we have assumed $\rho_B = \rho_{drip}$. Note, however, that for our evolutionary models we considered the case of $\rho_B = 0.9\rho_{drip}$ (see text for explanation).

4. THE STABILITY OF STRANGE DWARF STARS

We should note a very important property of SDs clearly different from the properties of WDs. Let us imagine that an SD with $\rho_B = \rho_{drip}$ suffers a tiny accretion. Then, ρ_B will increase, fulfilling $\rho_B \gtrsim \rho_{drip}$ and releasing dripped neutrons to be quickly burned (essentially in a weak interaction timescale $\sim 10^{-8}$ s) to SM. Let us assume that this event does not produce any kind of violent hydrodynamical process able to prompt some mass loss. Then, for a greater stellar mass, we shall have a star with a *larger* SM core, opposite to the requirements of equilibrium (GKW; see also Figs. 3 and 4). It will be clear below that such a configuration is not stable.

The instability of SD objects with $\rho_B = \rho_{drip}$ is also present in objects of constant mass as is clearly indicated by the results presented in Figure 6, in which the mass of the SM core for different choices of ρ_B for SD objects at constant mass is shown. If we have initially $\rho_B = \rho_{drip}$, any perturbation (e.g., radial pulsations) will force (at least for a while) ρ_B to increase and to drip some neutrons that, in turn, make the SM core grow. Then, if the structure is still in hydrostatic equilibrium, we must have $\rho_B \gtrsim \rho_{drip}$, so more neutrons will be dripped, which will make ρ_B grow still

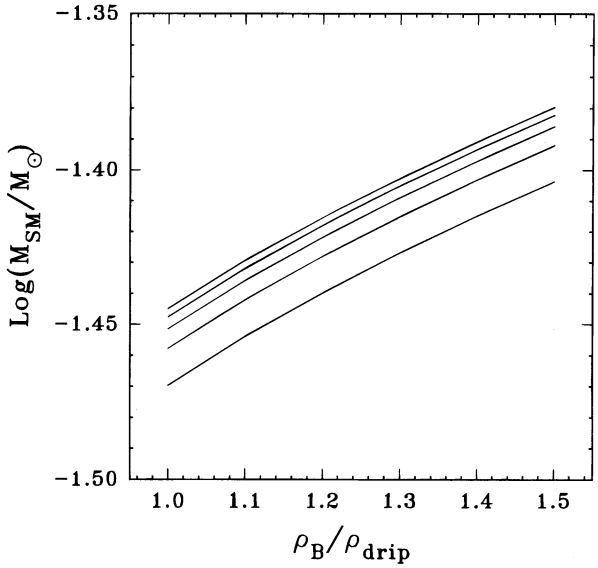

FIG. 6.—Mass of the SM core for different choices of ρ_B for SD objects of constant mass. The plotted sequences correspond, from bottom to top, to SD masses of 1.0, 0.8, 0.6, 0.4, and 0.2 $M_\odot$, respectively. See text for explanation.

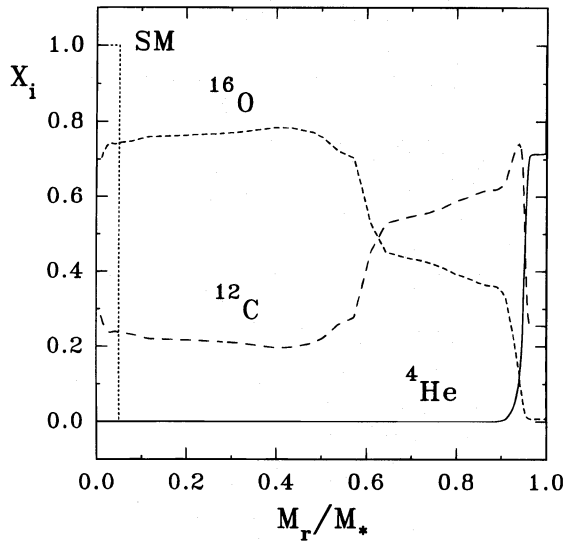

FIG. 7.—Chemical composition of models vs. the fractional mass. In the case of SD models, the approximate size of the SM core is denoted by a dotted line. For discussion of the composition of the high-density, normal matter layers in SDs (*not* included in this figure), see text.

further, and so on.[3] Thus, such a star will have no way to get another equilibrium structure as a SD resembling a WD but will burn dripped neutrons into SM continuously until it reaches the only available equilibrium structure as a (much more compact) SD resembling a SS (needless to say, such instability is not present if $\rho_B \lesssim \rho_{\rm drip}$). This event should release approximately the binding energy of a SS ($\sim 10^{53}$ ergs) in neutrino emission. Of course, such a high-energy release may produce a violent outcome.

Large differences between the behavior of SDs and WDs should be expected in close binary systems during the mass-exchanging stage. At such a stage, an accreting SD suffers a global compression, and in particular the dense, normal matter layers should fulfill $\rho_B \gtrsim \rho_{\rm drip}$. In this case, we expect some explosive phenomena because there are two energy sources that should begin to heat the SD interior simultaneously. One is the burning of dripped neutrons into SM, which should release about 20 MeV per particle (see, e.g., Farhi & Jaffe 1984) (and which also makes the SM core grow, destabilizing the structure, as discussed above), and the other is the pycnonuclear reactions (Salpeter & Van Horn 1969) that should also operate in the layers compressed to densities $\rho > 10^{10}$ g cm^{-3} that undergo crystallization as a result of the accretion. In this context, a stellar explosion resembling a faint Type Ia supernova should be expected.

5. THE CHEMICAL COMPOSITION OF STRANGE DWARF ENVELOPES

The problem of the chemical composition of the SD envelope is not a trivial one. We show in Figure 7 the composition of the low-density layers of SD (WD) models we employed (computed by D'Antona & Mazzitelli 1989 for a 0.55 $M_\odot$ WD model). In GKW, the Baym et al. (1971) EOS, which corresponds to nuclear statistical equilibrium, was employed. However, it is obvious in no way that this should be the actual case. In fact, stellar evolution predicts a carbon-oxygen–dominated interior as shown in Figure 7. Likewise, the maximum WD mass in equilibrium conditions is $M_{\rm WD}^{\rm max} \approx 1\ M_\odot$ (Shapiro & Teukolsky 1983) in strong contradiction with observations (Bergeron, Saffer, & Liebert 1992). Furthermore, the masses and radii of some WD objects observed in binary systems (Sirius B, 40 Eri B) are known with high accuracy; these observations are in contradiction with the theoretically predicted mass-radius relationship for an equilibrium composition, but not with a ^{12}C-^{16}O–dominated interior (see, e.g., Shapiro & Teukolsky 1983).[4] Accordingly, we expect a ^{12}C-^{16}O–dominated composition for $\rho \leq 10^9$ g cm^{-3} (i.e., the initially nonsolid layers).

Higher density *solid* layers ($\rho \geq 10^9$ g cm^{-3}) should undergo pycnonuclear reactions (Salpeter & Van Horn 1969). Because of the extremely steep dependence of the reaction rates upon density, these layers must have been burned in earlier evolutionary stages ($\log L/L_\odot > 0$). It is important to remark that, as the SD cools down, the crystallization front propagates outward (see § 7.2); then, a priori, one can think that such reactions should also propagate together with the solid front, but these reactions are negligible in the range of luminosities ($-5.5 \leq \log L/L_\odot \leq 0$) considered here because of the low density of the crystallizating layers. We show, in Figure 8, the dependence of the $^{12}C + {}^{12}C \rightarrow {}^{24}Mg$ (the most important reaction) upon density and temperature (see Shapiro & Teukolsky 1983).

It is worth noting that pycnonuclear reactions affect the structure of the star very little because they change the mean molecular weight per electron μ_e only a little. Thus, this kind of nuclear burning will be unable to propagate outward in the star as it is known to occur in the case of thermonuclear burning stars (e.g., just after the depletion of central hydrogen as the star leaves the main sequence).

[3] In fact, we would need to perform such an analysis asking for a constant baryon number instead of constant mass; however, this would introduce a negligible correction.

[4] However, we note that if we also include all the masses and radii estimated for *single* WD objects, such an agreement with a ^{12}C-^{16}O–dominated interior is lost in the scatter probably because of observational errors (see Koester & Chanmugam 1990, particularly their Fig. 2)

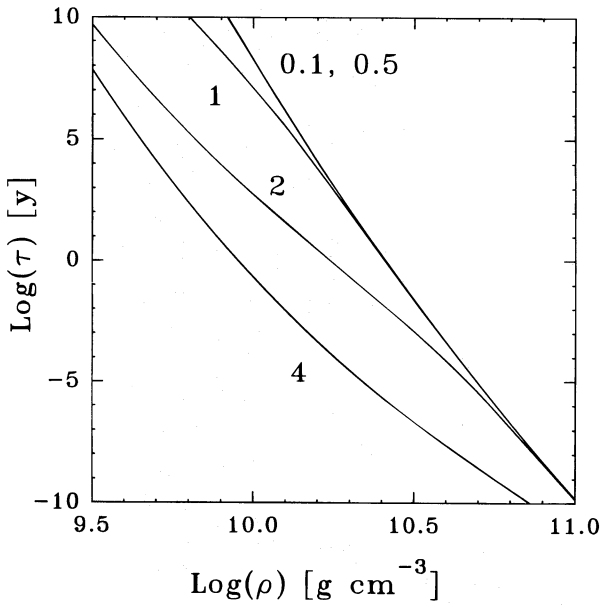

FIG. 8.—Half-lifetime of ^{12}C vs. density relationship due to pycnonuclear reactions at different temperatures. Each curve is labeled with T given in units of 10^8 K. Note that for $T = 10^7$ and 5×10^7 K, the curves are almost coincident.

The pycnonuclearly produced heavy elements are in a very thin shell of ~ 15 km thickness. This layer, which embraces a very small amount of matter ($\sim 2 \times 10^{-4}\ M_\odot$), retains so little heat that is unable to modify the SD cooling appreciably. Then, for type A SD models, we assumed the chemical composition profile of Figure 7, with a narrow layer composed of heavy elements as predicted by the Baym et al. (1971) EOS for $\rho \geq 10^9$ g cm^{-3}.

Nevertheless, the problem of SD envelope composition will be completely solved only when self-consistent stellar evolution computations consider the effects due to the presence of a compact SM core starting from the main sequence. So, in principle, it is still possible that for high densities (e.g., $\rho \gtrsim 10^7$ g cm^{-3}), previous evolution leads to nuclear statistical equilibrium (however, see § 8). Then, for the sake of completeness, we also considered type B SD models assuming the chemical composition of Figure 7 together with the predicted composition by the Baym et al. (1971) EOS for $\rho \geq 10^7$ g cm^{-3}.

6. THE NUMERICAL CODE

For the cooling calculations we used a WD evolutionary code (see Benvenuto & Althaus 1995a for description) modified to allow for the properties of the SM core given in § 2. General relativity corrections are at a maximum at the SM core surface, where we have

$$\frac{GM}{rc^2} \approx \left(\frac{2}{c^2}\right)\left(\frac{2\pi G P_c}{3}\right)^{1/2} \approx 10^{-2}\,, \qquad (16)$$

so that we can safely neglect these effects in our SD models and employ a well-tested WD evolutionary code.

For the EOS at finite temperature, necessary to compute the evolution of the objects in which we are interested, we employed the EOS described in Benvenuto & Althaus (1995a), which tends to the EOS given in Salpeter (1961) as $T \to 0$. Such a treatment leads at $T = 0$ to very tiny differences in pressure compared to the Baym et al. (1971) EOS. Such pressure differences are negligible in the study of the structure of our models (see Shapiro & Teukolsky 1983 for further details).

7. THE EVOLUTION OF STRANGE DWARF STARS

We have evolved SD models with masses of 0.4, 0.55, and 0.8 $M_\odot$ taking $\rho_B = \eta\rho_{\rm drip}$, provided $\eta < 1$ ($\eta = 0.9$ in this work) even at low luminosities. We note that η is not a critical parameter, and if $\eta \lesssim 1$, SD evolution will be essentially that presented below (we have verified this fact by computing the SD evolution for other values of η). We also evolved standard WD models for the same stellar masses. The range of masses considered in this work covers most of the observed WD distribution (at least for the case of H-rich envelopes, the so-called DA type; see Bergeron et al. 1992).

7.1. *The Initial Models*

For constructing SD initial models, we performed an integration of the stellar structure equations from the center up to low densities ($\rho \approx 10^5$ g cm^{-3}), and then, we superimposed the structure of WD lower density layers previously computed. In order to begin our evolutionary calculations at high luminosities, we heated the models performing an "artificial evolution" procedure described in Benvenuto & Althaus (1995a) (see Kippenhahn, Weigert, & Hofmeister 1967 for some other useful techniques). In broad outline, we have incorporated an artificial, constant specific energy release for the entire model, which has been increased progressively until the SD (WD) reaches a luminosity (approximately $\log L/L_\odot = 1$) far larger than that corresponding to the first model considered here. Then, we turned it off smoothly, fast enough to reach $L = L_\odot$ with no contribution of this artificial procedure. The transitory state of the SD (WD) interior is damped out, and we get a plausible initial structure for our SD (WD) models. For more details, see Benvenuto & Althaus (1995a).

7.2. *Numerical Results*

We have evolved SD and WD models in the range of luminosities from 1 $L_\odot$ to $10^{-5.5}$ $L_\odot$, where a wealth of observational data has been compiled. It allows us to perform a detailed comparison of our results with observations. The main evolutionary results are presented in Figures 9–14 and Tables 1–3.

The central and maximum temperatures versus the luminosity for the models here computed are shown in Figure 9. For the three types of models, and at a given luminosity, the higher the maximum temperature, the lower the mass. For $\log L/L_\odot \geq -2.5$, the central temperature of SDs is significatively lower compared to that of WDs of the same mass. However, for a given stellar mass, the maximum temperatures of SDs and WDs are almost coincident. The position of the maximum temperature in the Lagrangian coordinate versus the luminosity is shown in Figure 10. Note that for SDs the maximum temperature is off-center for luminosities significatively lower compared to WDs of the same mass. For all the models considered here, the maximum temperature reaches the center at higher luminosities, the higher the mass is. We also note that, because of the extremely high conductivity of SM (see eq. [2]), the compact core remains almost isothermal throughout the evolution of the SD models.

In Figure 11 we show the neutrino emission versus luminosity relationship of the models. In order to affect the

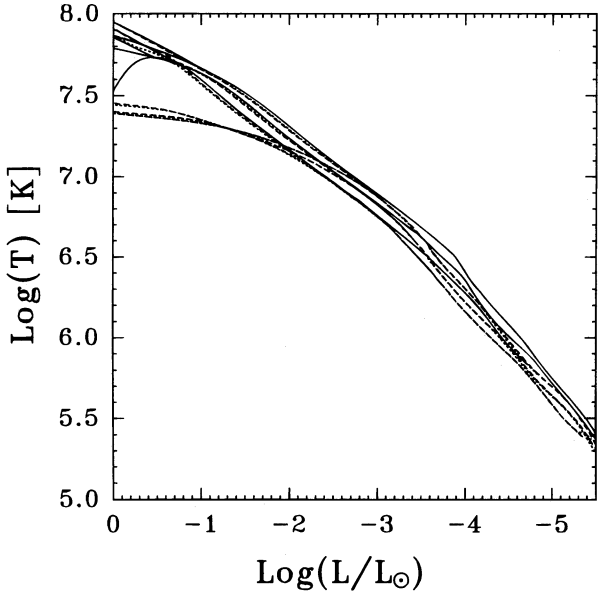

FIG. 9.—Central and maximum temperatures vs. the luminosity for type A SD, type B SD, and WD models correspond to medium-dashed, dotted, and solid lines, respectively. For the three kinds of models, for a given luminosity, the higher the maximum temperature, the lower the stellar mass. Note that for types A and B SD models at $\log L/L_\odot \geq -2$, the central temperature is significatively lower compared to WD models of the same mass. This is because of the strong neutrino emission of the compact SM core.

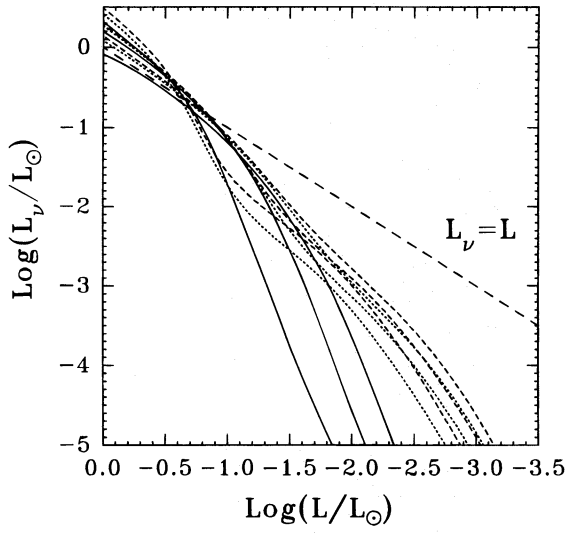

FIG. 11.—Neutrino emission vs. the luminosity of the models. The meanings of the different lines are as in Fig. 9. For the sake of reference, the line $L_\nu = L$ is also shown. Note that neutrino emission is the main cooling agent for $\log L/L_\odot \geq -0.8$. For lower luminosities, neutrinos are much less efficient than photons as a cooling mechanism. SDs suffer much stronger neutrino emission than WDs for $\log L/L_\odot \leq -1$ because of the presence of the compact SM core.

cooling significantly, neutrino emission should be comparable to photon emission. It is clear that neutrinos are the main agent of energy loss for most of models with $\log L/L_\odot \geq -0.8$ (with the only exception of the $0.4\,M_\odot$ WD model). At lower luminosities, neutrino emission fades away faster than photon emission (note in Fig. 11 that the slope of its decay is greater than 1). Quickly, neutrino losses become an order of magnitude lower than photon losses, thus having little effect on cooling times from then on. At these stages, in the case of type A and B SD models, neutrino emission is far more important than in WD models of the same mass and luminosity because of the presence of the compact SM core.

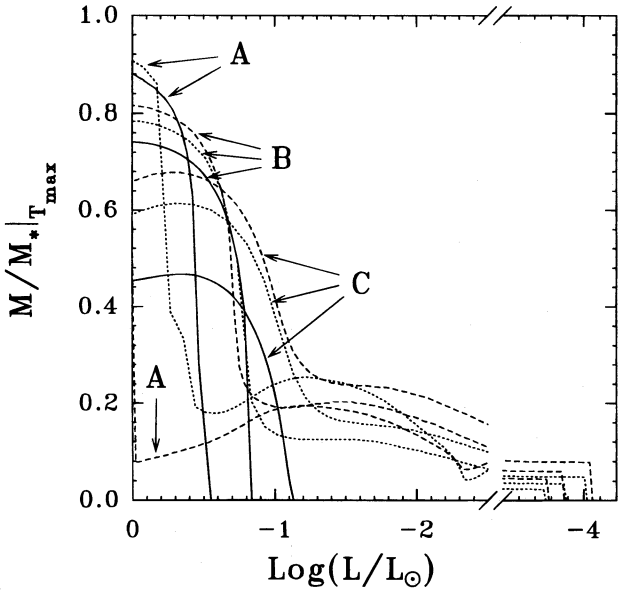

FIG. 10.—Position of the maximum temperature in the Lagrangian coordinate vs. the luminosity for type A SD, type B SD, and WD models. A, B, and C stand for 0.8, 0.55, and 0.4 $M_\odot$ models, respectively. The meanings of the different lines are as in Fig. 9. Note that for SD models the central temperature is still outside the center for luminosities significatively lower compared to WD models of the same mass. This is because of the strong neutrino emission of the compact SM core.

Another topic of interest is crystallization. It is well known that it affects the cooling in two ways: first, it releases some latent heat just at the phase transition, which retards the cooling; second, it modifies the specific heat (see, e.g., D'Antona & Mazzitelli 1990). Crystallization has been assumed to occur when the plasma coupling constant Γ reaches the value[5] $\Gamma_m = 160$, where

$$\Gamma \equiv \frac{Z^2 e^2}{kT\langle r\rangle} = 2.2697 \times 10^5 \frac{\rho^{1/3}}{T} \sum_i X_i Z_i^2 A_i^{-1/3}, \quad (17)$$

where $\langle r\rangle$ is the mean interparticle distance, and X_i is the abundance by mass of an ion of atomic mass A_i and charge Z_i.

We show the evolution of the crystallization front in the Lagrangian coordinate as a function of the luminosity for type A and type B SD, and WD models in Figure 12. For the three types of objects, the growth of the crystallized core begins at higher luminosities, the higher the stellar mass is. However, for a given stellar mass, SDs crystallize at higher luminosities than WDs because of their higher internal densities as is expected according to equation (17). Note that in the case of SDs a tiny amount of matter is in the crystal phase even at $L = L_\odot$ (see Tables 1, 2, and 3) because of the presence of the high-density layers surrounding the SM core. This is another interesting difference of SD compared

[5] Note, however, that this value is rather uncertain and, as discussed by Ichimaru, Iyetomi, & Mitake (1983), may be significantly higher ($\Gamma_m \approx 210$).

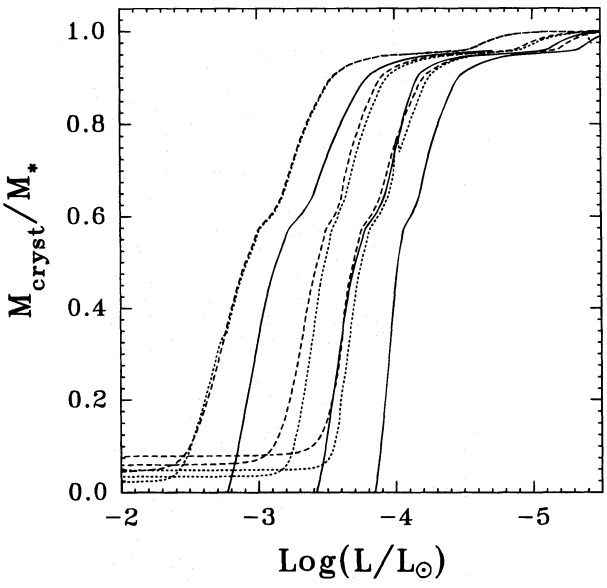

FIG. 12.—Evolution of the crystallization front in the Lagrangian coordinate as a function of the luminosity for type A SD, type B SD, and WD models. The meanings of the different lines are as in Fig. 9. For the three types of objects, the crystallized core begins to grow appreciably at higher luminosities, the higher the stellar mass is. However, for a given stellar mass, SDs crystallize at higher luminosities than WDs because of their higher internal densities.

to WD models that was important in the discussion of the effects of pycnonuclear reactions detailed in § 5 in relation to the chemical composition of these layers.

In Figure 13 we show the luminosity of the models versus their ages. In order to allow for a meaningful comparison of the different types of model ages, we have chosen to set the age t as $t = 0$ at $\log L/L_\odot = 0$. Concerning WDs, it is possible to compute the time the star has spent in reaching such a luminosity (pre-WD evolution). However, as quoted previously, this is not the case in SD models. The procedure we decided to adopt in this work is the simplest and, currently, the only one available in order to compare the ages of WD and SD models.

As can be realized from Figure 13, in spite of the large differences found in the behavior of the central part of SDs compared to WDs, the cooling curves are very similar. Perhaps the main difference is that SDs cool down a bit faster than WDs because of the combined effect of the stronger neutrino emission and lower specific heat. This is an important result that shows us that in order to differentiate SD from WD models, cooling calculations are not useful as can be imagined ab initio.

Of particular interest is the observed WD luminosity function (LF) (Liebert, Dahn, & Monet 1988), i.e., the number of stars per unit volume and per unit of magnitude, usually called Φ. Theoretically, in the case of constant birthrate, $\Phi \propto dt_{cool}/d \log (L/L_\odot)$ for a given stellar mass. In Figure 14 we show Φ as a function of $\log (L/L_\odot)$ for each WD, type A SD, and type B SD model (denoted as Φ_{WD}, Φ^A_{SD}, and Φ^B_{SD}, respectively) normalized at the observed value of $\Phi[\log (L/L_\odot) = -2.616] = -3.821$ pc^{-3} M_{bol}^{-1}. In this plot, for all the types of models at $\log (L/L_\odot) = 0; -4$, the larger the mass, the lower the Φ. As can be expected from the results of Figure 13, for a given mass, Φ^A_{SD}, Φ^B_{SD}, and Φ_{WD} are very similar, and the largest differences occur at very low luminosities, at which the objects are almost completely solid (see Fig. 12). At such low luminosities, the specific heat in most of the interior is $C_V \propto \rho^{-3/2} T^3$, which leads to a fast (Debye) cooling. Because, in the case of a SD, the density near the SM core is by far larger than for a WD of the same mass, in these layers $C_V^{SD} \ll C_V^{WD}$, which explains the slightly faster falling down of Φ^A_{SD} and Φ^B_{SD} compared to Φ_{WD}. However, unfortunately, at these low luminosities, the uncertainties on the observed LF are by far the largest, much larger than the differences between Φ^A_{SD}, Φ^B_{SD}, and Φ_{WD}, thereby preventing us from distinguishing SDs from

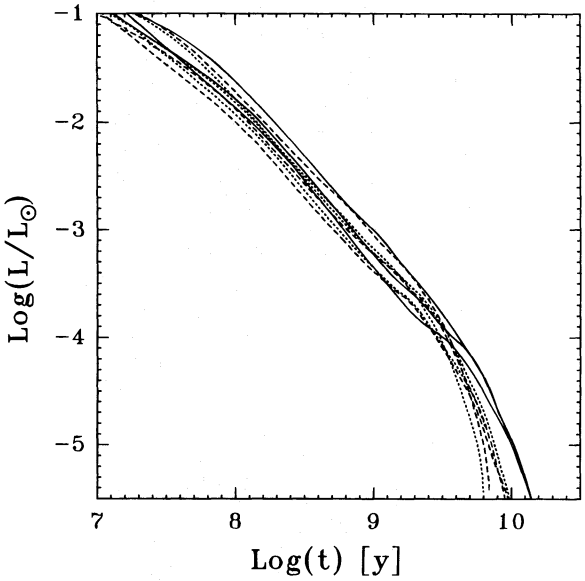

FIG. 13.—Luminosity of type A SD, type B SD, and WD models vs. their age. The meanings of the different lines are as in Fig. 9. For $\log L/L_\odot = -3$, type B SD and WD models the higher the mass, the greater their ages. At the same luminosity, for type A SD models the sequence of masses for increasing ages is 0.4, 0.8, and 0.55 $M_\odot$.

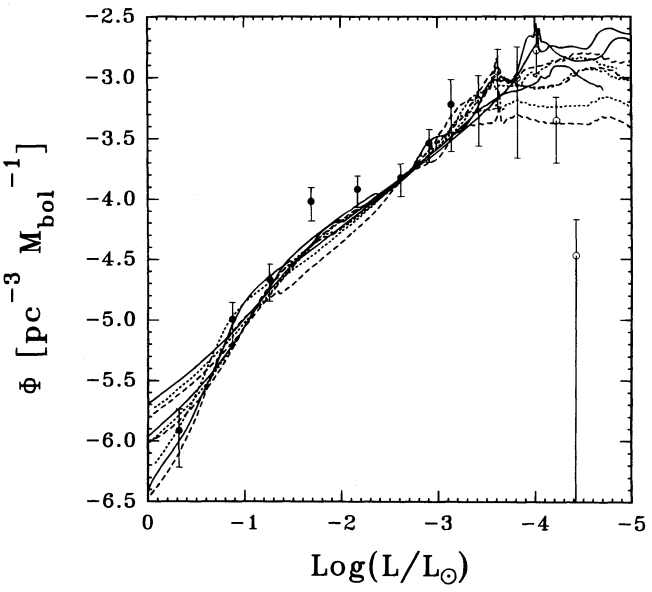

FIG. 14.—Theoretical luminosity function (for constant birthrate) vs. logarithm of the luminosity for type A SD, type B SD, and WD models. The meanings of the different lines are as in Fig. 9. The observed LF values with their respective error bars (Liebert et al. 1988) are also included. See text for explanation.

TABLE 1

SELECTED STAGES FOR A 0.4 $M_\odot$ TYPE A SD

log $L/L_\odot$	log $L_\nu/L_\odot$	log $T_{\rm eff}$	log T_c	log $T_{\rm max}$	$M(T_{\rm max})/M_*$	$M_{\rm cr}/M_*$	log Age
0.0.....	0.1474	4.660	7.394	7.949	0.6599	0.0781	$-\infty$
−0.1.....	0.0324	4.639	7.387	7.920	0.6692	0.0781	5.6725
−0.2.....	−0.0804	4.617	7.380	7.891	0.6753	0.0781	6.0043
−0.3.....	−0.1930	4.595	7.375	7.862	0.6774	0.0781	6.2121
−0.4.....	−0.3072	4.573	7.369	7.833	0.6741	0.0781	6.3709
−0.5.....	−0.4241	4.551	7.364	7.803	0.6649	0.0781	6.5035
−0.6.....	−0.5451	4.528	7.358	7.774	0.6488	0.0781	6.6214
−0.7.....	−0.6715	4.506	7.352	7.744	0.6223	0.0781	6.7296
−0.8.....	−0.8047	4.483	7.346	7.715	0.5798	0.0781	6.8326
−0.9.....	−0.9463	4.460	7.338	7.686	0.5136	0.0782	6.9325
−1.0.....	−1.0977	4.437	7.330	7.658	0.4186	0.0782	7.0313
−1.1.....	−1.2596	4.414	7.321	7.629	0.3264	0.0782	7.1303
−1.2.....	−1.4318	4.391	7.311	7.599	0.2766	0.0782	7.2301
−1.3.....	−1.6125	4.368	7.300	7.567	0.2531	0.0782	7.3308
−1.4.....	−1.7970	4.344	7.287	7.533	0.2422	0.0782	7.4316
−1.5.....	−1.9793	4.321	7.272	7.496	0.2382	0.0782	7.5315
−1.6.....	−2.1554	4.297	7.256	7.457	0.2363	0.0783	7.6313
−1.7.....	−2.3232	4.273	7.239	7.415	0.2339	0.0783	7.7313
−1.8.....	−2.4834	4.250	7.220	7.372	0.2317	0.0783	7.8265
−1.9.....	−2.6368	4.227	7.200	7.329	0.2252	0.0784	7.9158
−2.0.....	−2.7848	4.203	7.179	7.286	0.2172	0.0784	8.0009
−2.1.....	−2.9334	4.179	7.156	7.242	0.2079	0.0785	8.0814
−2.2.....	−3.0857	4.155	7.131	7.200	0.1953	0.0785	8.1578
−2.3.....	−3.2377	4.131	7.106	7.159	0.1830	0.0786	8.2276
−2.4.....	−3.3961	4.107	7.080	7.120	0.1701	0.0787	8.2947
−2.5.....	−3.5663	4.083	7.052	7.081	0.1567	0.0788	8.3616
−2.6.....	−3.7493	4.058	7.022	7.042	0.1441	0.0789	8.4284
−2.7.....	−3.9443	4.034	6.989	7.003	0.1305	0.0791	8.4953
−2.8.....	−4.1528	4.010	6.955	6.963	0.1185	0.0793	8.5632
−2.9.....	−4.3775	3.986	6.917	6.922	0.1083	0.0797	8.6326
−3.0.....	−4.6217	3.961	6.877	6.879	0.0988	0.0802	8.7045
−3.1.....	−4.8805	3.937	6.833	6.834	0.0903	0.0813	8.7773
−3.2.....	−5.1524	3.912	6.788	[a]	0.0841	0.0832	8.8506
−3.3.....	−5.4356	3.888	6.741	[a]	0.0857	0.0879	8.9250
−3.4.....	−5.7482	3.864	6.689	[a]	0.0840	0.1024	9.0053
−3.5.....	−6.1088	3.839	6.629	[a]	0.0819	0.1582	9.0956
−3.6.....	−6.5221	3.815	6.560	[a]	0.0804	0.3070	9.1909
−3.7.....	−6.9938	3.790	6.481	[a]	0.0794	0.5085	9.2788
−3.8.....	−7.3635	3.765	6.420	[a]	0.0789	0.5932	9.3360
−3.9.....	−7.7017	3.740	6.363	[a]	0.0787	0.6526	9.3920
−4.0.....	−8.0645	3.716	6.303	[a]	0.0784	0.7572	9.4474
−4.1.....	−8.4269	3.691	6.242	[b]	0.0000	0.8352	9.4986
−4.2.....	−8.7998	3.666	6.180	[b]	0.0000	0.8960	9.5466
−4.3.....	−9.1794	3.641	6.117	[b]	0.0000	0.9217	9.5914
−4.4.....	−9.5761	3.616	6.051	[b]	0.0000	0.9358	9.6359
−4.5.....	−9.9812	3.591	5.983	[b]	0.0000	0.9436	9.6781
−4.6.....	−10.3797	3.566	5.917	[b]	0.0000	0.9478	9.7168
−4.7.....	−10.7647	3.541	5.853	[b]	0.0000	0.9504	9.7519
−4.8.....	−11.1040	3.516	5.796	[b]	0.0000	0.9523	9.7815
−4.9.....	−11.4102	3.492	5.745	[b]	0.0000	0.9539	9.8077
−5.0.....	−11.7033	3.467	5.696	[b]	0.0000	0.9555	9.8326
−5.1.....	−12.0040	3.442	5.646	[b]	0.0000	0.9576	9.8582
−5.2.....	−12.3423	3.417	5.590	[b]	0.0000	0.9637	9.8869
−5.3.....	−12.7778	3.392	5.517	[b]	0.0000	0.9820	9.9199
−5.4.....	−13.2772	3.367	5.434	[b]	0.0000	0.9927	9.9505
−5.5.....	−13.8472	3.342	5.339	[b]	0.0000	0.9976	9.9773

[a] log $T_{\rm max}$ and log T_c differ only since the fourth decimal.
[b] The central temperature is the maximum one.

WDs. Also note that, for a given mass, the slopes of LFs in the neutrino-dominated epoch (log $L/L_\odot \geq -1$) are almost the same, showing that it is essentially independent of the SM neutrino emissivity.

We should mention that, in order to make a careful comparison between theoretical and observational LFs, we would have to perform an average of the constant-birthrate theoretical LFs (Wood 1992, eq. [2]) over, among other things, the stellar formation rate and the initial mass function. Such an average is fundamental if we want to compute the age of the galactic disk by adjusting the sudden drop of the observed LF at log $(L/L_\odot) \approx -4.5$ (see, e.g., Wood 1992; D'Antona & Mazzitelli 1990). Whatever the average we choose, it is obvious that we shall not be able to distinguish $\Phi^{\rm A}_{\rm SD}$ and $\Phi^{\rm B}_{\rm SD}$ from $\Phi_{\rm WD}$ if the error bars on the observed LF are larger than the differences between these two models for each stellar mass. This is indeed the case, as can be noticed from Figure 14. Consequently, even with the deep differences in the innermost structure and evolution of the three types of objects, provided $\rho_B < \rho_{\rm drip}$ even at

TABLE 2

SELECTED STAGES FOR A 0.55 $M_\odot$ TYPE A SD

log $L/L_\odot$	log $L_\nu/L_\odot$	log $T_{\rm eff}$	log T_c	log $T_{\rm max}$	$M(T_{\rm max})/M_*$	$M_{\rm cr}/M_*$	log Age
0.0.....	0.4724	4.716	7.426	7.917	0.7931	0.0594	$-\infty$
−0.1.....	0.2858	4.693	7.411	7.882	0.7988	0.0594	5.5757
−0.2.....	0.1311	4.670	7.402	7.849	0.7959	0.0594	5.8991
−0.3.....	−0.0107	4.647	7.395	7.818	0.7846	0.0594	6.1039
−0.4.....	−0.1485	4.624	7.388	7.789	0.7610	0.0594	6.2640
−0.5.....	−0.2876	4.600	7.382	7.760	0.7210	0.0594	6.4023
−0.6.....	−0.4326	4.577	7.376	7.733	0.6401	0.0594	6.5295
−0.7.....	−0.5875	4.554	7.369	7.709	0.2773	0.0594	6.6523
−0.8.....	−0.7561	4.530	7.361	7.687	0.2119	0.0594	6.7747
−0.9.....	−0.9420	4.506	7.353	7.662	0.1963	0.0595	6.8994
−1.0.....	−1.1471	4.483	7.342	7.633	0.1911	0.0595	7.0281
−1.1.....	−1.3676	4.459	7.330	7.599	0.1927	0.0595	7.1603
−1.2.....	−1.5958	4.435	7.316	7.561	0.1977	0.0595	7.2938
−1.3.....	−1.8161	4.411	7.300	7.520	0.2024	0.0595	7.4239
−1.4.....	−2.0123	4.387	7.282	7.476	0.2044	0.0596	7.5448
−1.5.....	−2.1823	4.363	7.264	7.433	0.2061	0.0596	7.6552
−1.6.....	−2.3368	4.339	7.245	7.389	0.2025	0.0596	7.7574
−1.7.....	−2.4825	4.314	7.224	7.344	0.1970	0.0597	7.8539
−1.8.....	−2.6248	4.291	7.203	7.301	0.1897	0.0597	7.9433
−1.9.....	−2.7634	4.266	7.180	7.259	0.1800	0.0598	8.0232
−2.0.....	−2.9028	4.242	7.158	7.220	0.1710	0.0599	8.0968
−2.1.....	−3.0524	4.217	7.133	7.181	0.1599	0.0600	8.1694
−2.2.....	−3.2123	4.193	7.107	7.141	0.1474	0.0601	8.2408
−2.3.....	−3.3847	4.169	7.078	7.102	0.1347	0.0602	8.3115
−2.4.....	−3.5702	4.144	7.047	7.063	0.1216	0.0605	8.3820
−2.5.....	−3.7680	4.120	7.014	7.024	0.1085	0.0608	8.4520
−2.6.....	−3.9771	4.095	6.979	6.985	0.0972	0.0613	8.5219
−2.7.....	−4.1952	4.071	6.943	6.946	0.0861	0.0622	8.5916
−2.8.....	−4.4213	4.046	6.905	6.906	0.0754	0.0639	8.6616
−2.9.....	−4.6565	4.022	6.866	6.866	0.0686	0.0675	8.7334
−3.0.....	−4.9077	3.997	6.824	6.824	0.0725	0.0778	8.8098
−3.1.....	−5.1892	3.973	6.777	6.778	0.0704	0.1129	8.8946
−3.2.....	−5.5015	3.948	6.725	[a]	0.0670	0.2027	8.9852
−3.3.....	−5.8355	3.923	6.670	[a]	0.0643	0.3483	9.0750
−3.4.....	−6.1802	3.899	6.612	[a]	0.0626	0.4958	9.1553
−3.5.....	−6.5350	3.874	6.553	[a]	0.0614	0.5855	9.2262
−3.6.....	−6.9346	3.849	6.487	[a]	0.0609	0.6504	9.3042
−3.7.....	−7.4083	3.824	6.407	[a]	0.0602	0.7791	9.3824
−3.8.....	−7.8089	3.800	6.341	[a]	0.0599	0.8571	9.4393
−3.9.....	−8.1939	3.775	6.277	[b]	0.0000	0.9080	9.4873
−4.0.....	−8.5444	3.750	6.218	[b]	0.0000	0.9258	9.5284
−4.1.....	−8.8791	3.725	6.162	[b]	0.0000	0.9366	9.5662
−4.2.....	−9.2023	3.700	6.109	[b]	0.0000	0.9427	9.6017
−4.3.....	−9.5155	3.675	6.056	[b]	0.0000	0.9467	9.6354
−4.4.....	−9.8397	3.650	6.002	[b]	0.0000	0.9490	9.6695
−4.5.....	−10.1944	3.625	5.943	[b]	0.0000	0.9513	9.7053
−4.6.....	−10.5745	3.600	5.880	[b]	0.0000	0.9533	9.7409
−4.7.....	−10.9605	3.575	5.816	[b]	0.0000	0.9554	9.7741
−4.8.....	−11.3422	3.550	5.752	[b]	0.0000	0.9581	9.8042
−4.9.....	−11.6986	3.525	5.692	[b]	0.0000	0.9667	9.8306
−5.0.....	−12.0305	3.500	5.637	[b]	0.0000	0.9804	9.8532
−5.1.....	−12.3495	3.475	5.584	[b]	0.0000	0.9885	9.8734
−5.2.....	−12.6767	3.450	5.529	[b]	0.0000	0.9935	9.8926
−5.3.....	−13.0356	3.425	5.470	[b]	0.0000	0.9966	9.9117
−5.4.....	−13.4823	3.400	5.395	[b]	0.0000	0.9985	9.9318
−5.5.....	−13.9793	3.375	5.312	[b]	0.0000	0.9988	9.9494

[a] log $T_{\rm max}$ and log T_c differ only since the fourth decimal.
[b] The central temperature is the maximum one.

$t \to \infty$, it seems impossible, with the currently available observational data, to distinguish SD from WD stars with this kind of study. Moreover, it is also impossible to distinguish between SDs of type A and B with the analysis performed above. However, it is important to note that the SM hypothesis is not in contradiction with the existence and the evolution of WD stars.

8. DISCUSSION AND CONCLUSIONS

We have studied the structure and evolution of strange dwarf (SD) stars. We restricted our analysis to the case of low–central pressure objects that have a mass-radius relation very similar to that corresponding to white dwarf (WD) stars.

SDs resembling WDs correspond to a very narrow range of central pressures. The almost discontinuous behavior of these structures with respect to changes of the central pressure was analyzed in the frame of a polytropic-like analysis, showing that the envelope of all these objects is nicely described by the Lane-Emden equation of $n = 3$ with the boundary conditions given by equations (11) and (14). In contrast to earlier expectations, we also show that SDs are

TABLE 3

SELECTED STAGES FOR A 0.8 $M_\odot$ TYPE A SD

log $L/L_\odot$	log $L_\nu/L_\odot$	log $T_{\rm eff}$	log T_c	log $T_{\rm max}$	$M(T_{\rm max})/M_*$	$M_{\rm cr}/M_*$	log Age
0.0.....	0.6905	4.786	7.470	7.909	0.0634	0.0436	$-\infty$
−0.1.....	0.4744	4.762	7.457	7.878	0.0715	0.0436	5.4498
−0.2.....	0.2935	4.738	7.448	7.852	0.0801	0.0436	5.7879
−0.3.....	0.1192	4.715	7.439	7.829	0.0881	0.0436	6.0156
−0.4.....	−0.0633	4.690	7.431	7.805	0.0984	0.0436	6.2090
−0.5.....	−0.2659	4.666	7.422	7.779	0.1110	0.0436	6.3925
−0.6.....	−0.5002	4.642	7.411	7.749	0.1240	0.0437	6.5796
−0.7.....	−0.7733	4.618	7.398	7.712	0.1408	0.0437	6.7768
−0.8.....	−1.0669	4.594	7.383	7.668	0.1576	0.0437	6.9738
−0.9.....	−1.3399	4.570	7.366	7.622	0.1757	0.0438	7.1519
−1.0.....	−1.5668	4.546	7.349	7.576	0.1859	0.0438	7.3050
−1.1.....	−1.7476	4.522	7.332	7.530	0.1924	0.0438	7.4362
−1.2.....	−1.8971	4.498	7.315	7.486	0.1941	0.0439	7.5510
−1.3.....	−2.0301	4.473	7.296	7.441	0.1926	0.0440	7.6541
−1.4.....	−2.1544	4.449	7.278	7.399	0.1900	0.0440	7.7452
−1.5.....	−2.2747	4.424	7.259	7.359	0.1852	0.0441	7.8275
−1.6.....	−2.4000	4.399	7.238	7.318	0.1798	0.0442	7.9077
−1.7.....	−2.5326	4.375	7.216	7.278	0.1714	0.0444	7.9864
−1.8.....	−2.6761	4.350	7.193	7.238	0.1606	0.0446	8.0634
−1.9.....	−2.8306	4.326	7.167	7.199	0.1481	0.0449	8.1382
−2.0.....	−2.9997	4.301	7.139	7.160	0.1331	0.0454	8.2121
−2.1.....	−3.1825	4.277	7.109	7.121	0.1180	0.0463	8.2853
−2.2.....	−3.3791	4.252	7.076	7.081	0.0994	0.0482	8.3583
−2.3.....	−3.5866	4.227	7.041	7.043	0.0724	0.0525	8.4312
−2.4.....	−3.8043	4.203	7.005	7.006	0.0664	0.0645	8.5052
−2.5.....	−4.0344	4.178	6.967	[a]	0.0770	0.0985	8.5822
−2.6.....	−4.2852	4.153	6.925	[a]	0.0709	0.1705	8.6628
−2.7.....	−4.5423	4.128	6.882	[a]	0.0647	0.2723	8.7441
−2.8.....	−4.8049	4.104	6.838	[a]	0.0587	0.3918	8.8225
−2.9.....	−5.0650	4.079	6.795	[a]	0.0548	0.4926	8.8945
−3.0.....	−5.3287	4.054	6.751	[a]	0.0516	0.5692	8.9618
−3.1.....	−5.6041	4.029	6.705	[a]	0.0498	0.6046	9.0294
−3.2.....	−5.9139	4.005	6.653	[a]	0.0483	0.6668	9.1057
−3.3.....	−6.2623	3.980	6.596	[a]	0.0467	0.7575	9.1816
−3.4.....	−6.6145	3.955	6.537	[a]	0.0458	0.8279	9.2497
−3.5.....	−6.9645	3.930	6.478	[a]	0.0451	0.8841	9.3101
−3.6.....	−7.3204	3.905	6.419	[a]	0.0447	0.9150	9.3642
−3.7.....	−7.7235	3.881	6.352	[a]	0.0442	0.9316	9.4191
−3.8.....	−8.1049	3.856	6.288	[b]	0.0000	0.9407	9.4661
−3.9.....	−8.4948	3.831	6.223	[b]	0.0000	0.9463	9.5096
−4.0.....	−8.8605	3.806	6.162	[b]	0.0000	0.9490	9.5469
−4.1.....	−9.2039	3.781	6.105	[b]	0.0000	0.9512	9.5798
−4.2.....	−9.5295	3.756	6.051	[b]	0.0000	0.9530	9.6094
−4.3.....	−9.8469	3.731	5.998	[b]	0.0000	0.9547	9.6369
−4.4.....	−10.1580	3.706	5.946	[b]	0.0000	0.9565	9.6628
−4.5.....	−10.4627	3.681	5.895	[b]	0.0000	0.9592	9.6871
−4.6.....	−10.7733	3.656	5.844	[b]	0.0000	0.9684	9.7101
−4.7.....	−11.1199	3.631	5.786	[b]	0.0000	0.9814	9.7340
−4.8.....	−11.4988	3.606	5.723	[b]	0.0000	0.9900	9.7574
−4.9.....	−11.8986	3.581	5.656	[b]	0.0000	0.9949	9.7786
−5.0.....	−12.3102	3.556	5.587	[b]	0.0000	0.9975	9.7971
−5.1.....	−12.7107	3.531	5.521	[b]	0.0000	0.9988	9.8121
−5.2.....	−13.0555	3.506	5.463	[b]	0.0000	0.9988	9.8233
−5.3.....	−13.3621	3.481	5.412	[b]	0.0000	0.9988	9.8324
−5.4.....	−13.6638	3.456	5.362	[b]	0.0000	0.9988	9.8406
−5.5.....	−13.9849	3.431	5.308	[b]	0.0000	0.9988	9.8486

[a] log $T_{\rm max}$ and log T_c differ only since the fourth decimal.
[b] The central temperature is the maximum one.

stable only if the density at the bottom of the normal matter envelope is lower than that of neutron drip.

Because of the lack of computations of the previous evolution of SD objects, we assumed for the normal matter envelope a carbon-oxygen–dominated composition up to a density ρ of $\rho = 10^9$ g cm^{-3}, type A models ($\rho = 10^7$ g cm^{-3}, type B models). For higher densities we assumed nuclear statistical equilibrium according to the Baym et al. (1971) equation of state. It should be noted that, because of the presence of a compact strange matter core (which is very efficient at emitting neutrinos), the central parts of the star should also be much cooler compared to the standard case without such a compact core. This effect should modify the thermonuclear burning stages of the pre-SD evolution, inhibiting the occurrence of high-temperature reactions and thus the formation of heavy isotopes in this way.

We have computed the evolution of SDs of 0.4, 0.55, and 0.8 $M_\odot$ in the range of luminosities usually attributed to WDs. We show the central and maximum temperature (and its position in the Lagrangian coordinate), neutrino emis-

sion, crystallization profile, ages, and the luminosity function as a function of the stellar luminosity for each type of model and each stellar mass. It is clear from Figures 9–14 and Tables 1–3 that the central evolution is deeply different from that corresponding to WDs. This is because of two effects related to the presence of the compact strange matter core. First, it compresses the neighboring matter, which induces the change of chemical composition and specific heat in these layers. Second, neutrino emission from the compact core makes the core much cooler than the surrounding outer layers, even at low luminosities, in clear contrast with the WD case.

In spite of these large differences in the central evolution, we found that, if the density at the base of the normal matter envelope is slightly lower than the density of neutron drip, these objects have a luminosity function observationally indistinguishable from that corresponding to WDs. This is independent of the chemical composition of the normal matter, high-density layers and is the main conclusion of the present work.

However, SDs should behave very differently from WDs in mass-exchanging close-binary systems. This should indeed be the case because dripped neutrons are quickly burned to strange matter and also pycnonuclear reactions heat the interior. Then, we expect an energetic event like a Type Ia supernova. This event may in principle be suffered by a SD of *any* mass, in clear contrast to the behavior of WDs, for which such an event is expected only for objects near the Chandrasekhar mass. Because the mass of the exploding SD may be lower than 1.4 $M_\odot$, we expect a dimmer event. This may be a better signal in searching for SDs than that coming from the cooling. This topic surely deserves more attention.

Finally, we note that in this paper, as well as in the previous ones (GKW), we have assumed that SM does not have any bound state at some critical baryon number A. This intriguing possibility is not ruled out either by theory or by experiments. Michel (1988) proposed the possible existence of Q_α particles. This particle, if exists, has 6u + 6d + 6s quarks in the lowest, closed shell configuration, resembling the nucleus of helium. If this configuration indeed exists, there is no reason to limit the density at the bottom of the envelope, and SDs would still be possible configurations. However, in this case the strong constraint $\rho_B < \rho_{\rm drip}$ is relaxed, avoiding the possibility of catastrophic burning discussed above.

We acknowledge the partial financial support received from the University of La Plata, CIC, and PROFOEG (CONICET). We would also like to thank Professor N. K. Glendenning for sending us his referred papers before publication and also an anonymous referee for his (her) report that allowed us to improve the original version of this paper.

REFERENCES

Alcock, C., & Olinto, A. 1988, Ann. Rev. Nucl. Part. Sci., 38, 161
Baym, G., Pethick, C., & Sutherland, P. 1971, ApJ, 170, 299
Benvenuto., O. G., & Althaus, L. G. 1995a, Ap&SS, in press
———. 1995b, Phys. Rev. D, in press
Benvenuto, O. G., & Horvath, J. E. H. 1989, Phys. Rev. Lett., 63, 716
Benvenuto, O. G., Horvath, J. E., & Vucetich, H. 1989, Int. J. Mod. Phys., A4, 257
———. 1991, Int. J. Mod. Phys., A6, 4769
Benvenuto, O. G., & Lugones, G. 1995, Phys. Rev. D, 50, 6100
Bergeron, P., Saffer, R. A., & Liebert, J. 1992, ApJ, 394, 228
Chakrabarty, S., Raha, S., & Sinha, B. 1989, Phys. Lett. B, 229, 113
Chandrasekhar, S. 1939, An Introduction to the Study of Stellar Structure (Chicago: Univ. of Chicago Press)
———. 1964, Phys. Rev. Lett., 12, 114
D'Antona, F., & Mazzitelli, I. 1989, ApJ, 347, 934
———. 1990, ARA&A, 28, 139
Farhi, E., & Jaffe, R. L. 1984, Phys. Rev. D, 30, 2379
Glendenning, N. K., Kettner, Ch., & Weber, F. 1995a, ApJ, 450, 253 (GKW)
———. 1995b, Phys. Rev. Lett., 74, 3519
Haensel, P. 1991, Nucl. Phys. B (Proc. Suppl.), 24, 23
Heiselberg, H., & Pethick, C. J. 1993, Phys. Rev. D, 48, 2916
Horvath, J. E., Benvenuto, O. G., & Vucetich, H. 1992, Phys. Rev. D, 45, 3865
Ichimaru, S., Iyetomi, M., & Mitake, S. 1983, ApJ, 265, L83
Kippenhahn, R., Weigert, A., & Hofmeister, E. 1967, Meth. Comput. Phys., 7, 129
Koester, D., & Chanmugam, G. 1990, Rep. Prog. Phys., 53, 837
Lee, K. S., & Heinz, U. 1993, Phys. Rev. D, 47, 2068
Liebert, J., Dahn, C., & Monet, D. 1988, ApJ, 332, 891
Lugones, G., & Benvenuto, O. G. 1995a, Phys. Rev. D, in press
———. 1995b, Phys. Rev. D, submitted
Lugones, G., Benvenuto, O. G., & Vucetich, H. 1994, Phys. Rev. D, 51, 1989
Madsen, J., & Haensel, P., ed. 1991, Nucl. Phys. B, 24 (Proc. Suppl.)
Michel, F. C. 1988, Phys. Rev. Lett., 60, 677
Olesen, M. L., & Madsen, J. 1994, Phys. Rev. D, 49, 2698
Oppenheimer, J. R., & Volkoff, G. M. 1939, Phys. Rev., 55, 374
Salpeter, E. E. 1961, ApJ, 134, 669
Salpeter, E. E., & Van Horn, H. M. 1969, ApJ, 155, 183
Shapiro, S. L., & Teukolsky, S. A. 1983, Black Holes, White Dwarfs, and Neutron Stars: The Physics of Compact Objects (New York: J. Wiley & Sons)
Witten, E. 1984, Phys. Rev. D, 30, 272
Wood, M. A. 1992, ApJ, 386, 539